ELSEVIER

Journal of Membrane Science 148 (1998) 257–271

journal of MEMBRANE SCIENCE

Membrane-moderated stripping process for removing VOCs from water in a composite hollow fiber module

A. Das, I. Abou-Nemeh, S. Chandra[1], K.K. Sirkar*

Department of Chemical Engineering, Chemistry and Environmental Science, New Jersey Institute of Technology, Newark, NJ 07102, USA

Accepted 15 June 1998

Abstract

The ''stripmeation'' process for removing volatile organic compounds (VOCs) from water has been introduced and studied. An aqueous solution of the VOC is passed through the bores of hydrophobic microporous polypropylene hollow fibers having a plasma polymerized silicone coating on the fiber outside diameter; a vacuum is maintained on the shell side of the fiber. The VOC is stripped into the gas-filled pores of the hydrophobic substrate, permeates through the nonporous silicone skin and is recovered by condensation of the shell-side permeate stream. Removal of trichloroethylene (TCE) present in a concentration range 200–1040 ppm has been studied at 25°C. Process performance has been obtained over a range of flow rates. The observed TCE permeation and removal behavior has been modeled using a resistances-in-series approach; the two important resistances are the tube-side aqueous boundary layer resistance and the vapor permeation resistance of TCE through the silicone coating. Employing the known Graetz solution for the tube-side flow and the measured vapor permeation resistance of TCE, values of the overall TCE mass-transfer coefficient have been obtained. These values compare well with the experimental values. The conventional pervaporation process where the liquid feed solution is in contact with the nonporous silicone membrane has also been studied by passing the feed on the shell side. The tube-side feed-based operation performs much better than the shell-side based operation.

Keywords: Pervaporation; Hollow fiber membranes; Composite membranes; Mass transfer; Trichloroethylene

1. Introduction

This paper is concerned with removing volatile organic compounds (VOCs) from an aqueous solution by a membrane permeation process. Specifically, the aqueous solution is obtained from surfactant-enhanced aquifer remediation (SEAR) processes wherein an appropriately formulated micellar aqueous solution of a suitable surfactant is pumped underground to remove and recover nonaqueous phase liquids (NAPLs) that contaminate soil and groundwater in many hazardous sites. Such NAPLs primarily consist of VOCs like benzene, toluene, xylene, trichloroethylene (TCE), perchloroethylene (PCE), trichloroethane (TCA), etc. Therefore, application of a conventional pervaporation process using organophilic membranes is expected to be an effective technique to achieve this goal [1–4]. Further, hollow-fiber based

*Corresponding author. Tel.: +1-973-596-8447; fax: +1-973-596-8436; e-mail: sirkar@admin.njit.edu

[1]Currently at Air Products, Inc., Allentown, PA, USA.

0376-7388/98/$ – see front matter
PII: S0376-7388(98)00167-7

membrane devices are expected to provide a highly compact structure for such an operation in sites to be remediated.

The hollow fiber membranes of interest are hydrophobic microporous polypropylene fibers having a plasma polymerized nonporous silicone layer on the outside diameter of the fiber. Conventionally, one may wish to run the aqueous feed on the shell side where the mass-transfer coefficient can be considerably higher than that in the tube side [4,5]. This mode of pervaporation operation will however have significant permeate side pressure drop in the fiber bore [6], and in the porous substrate. The effect of the latter has been considered by Huang and Feng [7]. Shell-side feed in the hollow fiber of interest encounters as a separate problem in SEAR processes. The NAPLs are often contaminated by the heavy oils. Shell-side operation will lead to the permeation of these heavy oils through the nonporous rubbery skin into the microporous substrate. The permeated oils will create a severe permeate side pressure drop problem in pervaporation by partially or totally blocking substrate pores as well as the fiber bores.

Tube-side feed mode of operation will, however, have no such problem. The permeated oils can be removed through thousands of inter-fiber gaps just as the permeate vapor can be removed. However, there is considerable possibility that these heavy oils may form an immobilized liquid membrane in the substrate pores on the feed side. This may increase the selectivity of the VOC over water substantially. Such a phenomenon was deliberately created by Yang et al. [8] who had employed a contained nonvolatile organic liquid membrane in contact with a silicone capillary for pervaporation removal of toluene and TCE from water. The organic liquid membrane reduced the water flux by 3–5 times. Tube-side feed mode of the operation with the composite membrane in the present study is, however, possible only if the skin can handle the applied pressure difference. This is easily achieved in the particular membrane employed in this study.

Earlier studies of the tube-side feed mode of pervaporation operation generally employed homogeneous capillaries [4,9]. Composite hollow fibers of the type studied here create new process conditions. The surfactant-containing solution may or may not wet the polypropylene substrate pores. If the pores are not wetted, the pores will be gas filled. Any VOC in the water will be stripped into the gas-filled pore and will then be permeated through the silicone skin subjected to vacuum on the shell side (Fig. 1) via vapor permeation. This is not conventional pervaporation since the liquid feed is not in direct contact with the VOC-selective plasma polymerized silicone membrane layer. It is akin to the process of evapomeation [10,11] and may be termed more correctly as

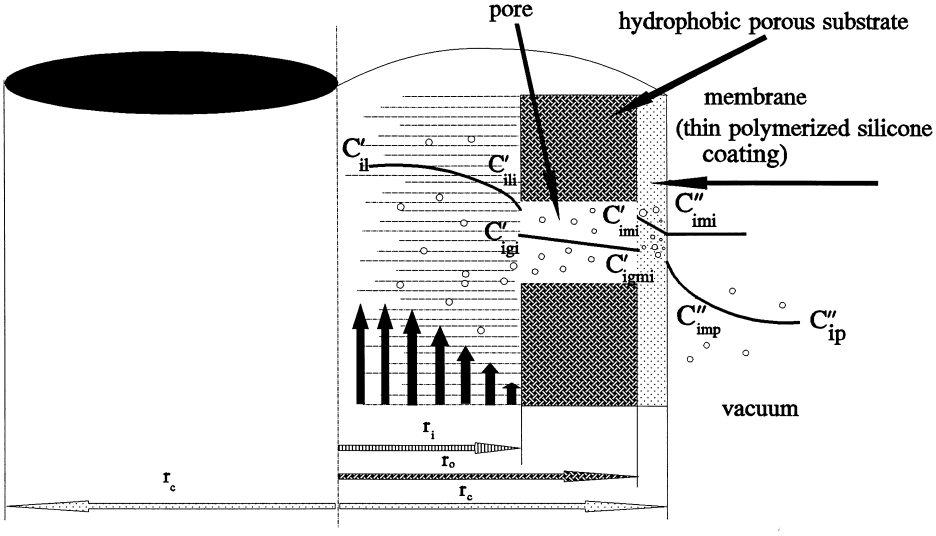

Fig. 1. Concentration profile of a VOC in a hollow fiber membrane-based stripmeation process.

''stripmeation''. In fact, it combines locally stripping and vapor permeation.

There is a considerable body of work (e.g., the work by Semmens et al. [12] and related hydrophobic microporous membrane-based stripping work) where a very dilute aqueous solution of VOC is on one side of the membrane and air or vacuum is on the other side. These processes are identified routinely in the literature as membrane-based ''air stripping'' or ''vacuum stripping''. In the process described here, we have an additional silicone membrane layer at the end of the pores through which vapor permeation occurs. Hence, the process is identified as ''stripmeation''. In conventional microporous membrane-based stripping, the pore contains water vapor also. In the present case air absorbed in the feed liquid is being stripped into the pore (just as in microporous membrane-based vacuum stripping) and then is permeated through the silicone membrane; Henry's law is used to describe the partitioning of air between water and the pore. Similarly, Henry's law will be used here to describe the partitioning of the VOC between the water and the pore. The basic separation and transport characteristics of such a process are studied here experimentally. We focus here on an aqueous solution of TCE without any surfactants. In Part II of the series, the treatment of surfactant-containing solutions of the VOC, TCE, will be considered. Part III will consider pilot plant results with an actual surfactant-flushed water from a contaminated site.

We illustrate here the performance of the composite hollow fiber membranes in removing TCE from water. The TCE concentration was varied from 200 to about 1040 ppm. We have studied the effects of TCE concentration and the fiber bore Reynolds number on the solute removal, the solute mass-transfer coefficient and the membrane selectivity. We have analyzed the various components of the overall mass-transfer resistance in this process and provided a basis for justifying the observed value of the overall solute mass-transfer coefficient.

2. Resistances-in-series model for the overall mass-transfer coefficient

Consider Fig. 1 which illustrates the solute concentration profiles in the aqueous solution, the gas-filled pore in the hydrophobic microporous substrate, the ultrathin silicone membrane on the fiber outside the diameter and the vacuum region present on the shell side. There are three phase interfaces (aqueous–pore gas; pore gas–silicone membrane; silicone membrane–vacuum side) and four resistances (tube-side aqueous boundary layer; gas-filled pore; silicone membrane; vacuum-side boundary layer).

Define three partition coefficients for the three phase interfaces:

$$C'_{ili} = H_i C'_{igi}, \tag{1}$$

$$C'_{imi} = m_{vf} C'_{igmi}, \tag{2}$$

$$C''_{imp} = m_{vp} C''_{imi}. \tag{3}$$

The molar rate of transfer of species i per unit length, R_i, may be expressed in terms of an overall mass-transfer coefficient K_o as well as four individual mass-transfer coefficients as follows:

$$R_i = K_o \pi d_o (C'_{il} - C''_{ipl}), \tag{4}$$

where C''_{ipl} is a hypothetical liquid phase concentration in equilibrium with the vacuum side gas phase concentration of C''_{ip}. The individual transfer coefficients may be defined by:

aqueous boundary layer:

$$R_i = k_l^f \pi d_i (C'_{il} - C'_{ili}), \tag{5}$$

gas-filled pore:

$$R_i = k_{gp}^f \pi d_{lm} (C'_{igi} - C'_{igmi}), \tag{6}$$

silicone membrane:

$$R_i = k_m \pi d_o (C'_{imi} - C''_{imi}), \tag{7}$$

vacuum boundary layer:

$$R_i = k_g^p \pi d_o (C''_{imp} - C''_{ip}). \tag{8}$$

There will be an additional interfacial resistance at the aqueous solution–pore gas interface if surfactants are present in the system. We have not considered any such resistance due to a monomolecular surfactant layer here since surfactants are absent in the system studied in this paper.

At steady state, the R_i's through all of the resistances-in-series are equal to one another and to that in

Eq. (4). We can therefore obtain

$$\frac{1}{K_o d_o} = \frac{1}{K_l^f d_i} + \frac{H_i}{k_{gp}^f d_{lm}} + \frac{H_i}{m_{vf} k_m d_o} + \frac{H_i}{k_g^p m_{vf} m_{vp} d_o}. \tag{9}$$

We assume the resistance of the vacuum side boundary layer to be negligible compared to others [8]. We are left with

$$\frac{1}{K_o} = \frac{d_o}{d_i}\frac{1}{k_l^f} + \frac{d_o}{d_{lm}}\frac{H_i}{k_{gp}^f} + \frac{H_i}{m_{vf} k_m}. \tag{10}$$

Of these, it may be easily demonstrated that the mass-transfer coefficient for the gas-filled pore is very large and the corresponding resistance may be neglected in comparison with the other terms:

$$\frac{H_i}{k_{gp}^f} = H_i \Big/ \left(\frac{D_{igp}\epsilon}{\delta_S \tau}\right) \cong 2.75 \Big/ \left(\frac{0.01069 \times 0.4}{2.5 \times 10^{-3} \times 2.49}\frac{\text{cm}}{\text{s}}\right) = 3.99\,\text{s/cm}. \tag{11}$$

Here D_{igp}, the diffusion coefficient of the solute in the pore gas phase, is based on slip flow and is obtained from [13]:

$$D_{igp} = 1.0133 \times 10^6 r_p \frac{RT}{M_i \bar{c}_i}, \tag{12a}$$

where $\bar{c}_i$, the mean speed of the molecule, is given by

$$\bar{c}_i = \left(8.1064 \times 10^6 \frac{RT}{\pi M_i}\right)^{1/2}. \tag{12b}$$

Callahan [14] had independently determined experimentally that gas transport through Celgard® membrane pores under ambient conditions behave such that the selectivity ratio for two species A and B is given by $(M_B/M_A)^{1/2}$, exactly as suggested by Eq. (12a). Under ambient conditions, the ratio of the Celgard® pore radius to the mean free path is around 0.3; this justifies the type of diffusion coefficient and the flux expression used here. The value of H_i, Henry's law constant as per Eq. (1), is obtained as 2.75 $(\text{mg/l})_{\text{liq}}/(\text{mg/l})_{\text{vap}}$ from Turner et al. [15]. δ_s is the fiber substrate thickness given by $[(290-240)/2]\,\mu\text{m} = 2.5\times10^{-3}$ cm. Since the observed values of the overall mass-transfer coefficient K_o is in the range 10^{-4} cm/s we can neglect the gas-filled pore resistance in Eq. (10) leaving us with

$$\frac{1}{K_o} = \frac{d_o}{d_i}\frac{1}{k_l^f} + \frac{H_i}{m_{vf} k_m}. \tag{13}$$

Since the mass-transfer behavior in laminar flow through the fiber bore is relatively well defined, experimental measurement of the solute vapor permeation transfer coefficient through the nonporous silicone coating ought to allow us to calculate the value of K_o which may then be compared with the experimentally obtained K_o. Our experimental strategy therefore includes separate determination of the vapor permeation-based removal of TCE from N_2 through the silicone membrane when both sides have gaseous phases and no liquid phase. It must be noted here that the value of k_l^f here corresponds to a somewhat variable boundary condition, namely, the TCE concentration at the surface of the microporous membrane changes along the fiber length. The solutions that are available for the tube-side laminar flow mass transfer with developing concentration boundary layer correspond to constant wall flux or constant wall concentration [16]; the corresponding limiting values of the Sherwood number at very low Graetz numbers are 4.36 and 3.56, respectively. This will introduce some uncertainty in the estimates of k_l^f to be used in Eq. (13) to calculate K_o.

The expression for Sherwood number for laminar fully developed velocity profile in a tube of length l with constant wall concentration is given by the expression [16]:

$$Sh|_{lm} = \frac{k_l^f d_i}{D_{il}} = \frac{1}{4}\left(\frac{d_i}{l}\right) Re\, Sc \times \ln\left[\sum_{j=1}^{j=\infty} \frac{-4B_j}{\beta_j^2}\left(\frac{d\phi_j}{dr_+}\right)_{r_+=1} \exp\left(\frac{-\beta_j^2 (x/r_t)}{Re\, Sc}\right)\right]^{-1}. \tag{14}$$

Note that this is based on the logarithmic-mean concentration difference over the whole tube. We calculate the value of k_l^f from Eq. (14) for substitution in Eq. (13).

3. Experimental

3.1. Chemicals and gases used

Trichloroethylene (purity 99.9%, FW 131.39, density 1.456 g/cm^3), acetonitrile (HPLC grade, purity 99.9%), methanol (purity 99.9%, FW 32.04), from Fischer Scientific (Springfield, NJ); ultrapure nitrogen, helium, air and liquid carbon dioxide from Matheson (E. Rutherford, NJ).

3.2. Hollow fiber membrane modules

The hollow fiber membrane modules contained hydrophobic microporous hollow fiber substrate (240 μm/290 μm ID/OD; polypropylene Celgard X-10, Hoechst Celanese, Charlotte, NC) having a plasma polymerized thin nonporous silicone skin on the outer surface. Three modules were prepared. The geometrical characteristics of only one of these modules used for the experiments are given in Table 1. Other modules were used in Part II. Detailed fabrication procedure is provided in [17].

3.3. Experimental setup

The setup for pervaporation is shown schematically in Fig. 2. Feed was pumped into the module by a peristaltic Masterflex pump, model 7518-10 (Cole-Parmer, Vernon Hills, IL) from a collapsible teflon bag (Cole-Parmer, Vernon Hills, IL). Teflon bags of two different sizes 1.2 l and 4.7 l were used depending on the flow rate and the duration of the experiment. Transparent 1/4 in. ID teflon tubing (Cole-Parmer, Vernon Hills, IL) and stainless steel fittings (Swagelok, R.S. Crum, New Brunswick, NJ) were used for the feed and all connecting lines to and from the membrane module. The feed line was connected to a three way valve (Swagelok, R.S. Crum, New Brunswick, NJ) for the collection of feed samples. A micrometering valve (Swagelok, R.S. Crum, New Brunswick, NJ) was connected to the feed line to regulate the feed pressure. An oil-less vacuum pump (KNF Neuberger, Trenton, NJ, Model UN 726.112 FTP) was used to maintain a vacuum of −28.5/−29.0 in. Hg. The permeate pressure was controlled by a Digital Vacuum Regulator Model 2000 (J-Kem Scientific, St. Louis, MO). Convoluted teflon tubes (Cole-Parmer, Vernon Hills, IL) were used for vacuum line connections to the condensers. The modules were immersed in a polyethylene water bath interfaced to a thermostat (Fisher Scientific, Springfield, NJ) to maintain the desired temperature range between 18°C and 50°C. All experiments for Part I of the series were run at 25°C. Two condensers (Labglass, Vineland, NJ) with a graduated tip were connected in series to the vacuum line before the vacuum pump. Dry ice and methanol were used as cooling medium in a Dewar flask (Labglass, Vineland, NJ), inside which each condenser was kept to trap the permeate vapor from the module outlet.

3.4. Analytical procedure

Aqueous TCE concentration was measured in a HP 6890 series gas chromatograph (GC) using a HP 7694 headspace sampler and HP 6890 series integrator (Hewlett Packard, Wilmington, DE). TCE was analyzed by a flame ionization detector (FID) using a HP-5 capillary column (crosslinked 5% PH ME siloxane) of 30 m length, 320 μm diameter and 1 μm film thickness (Hewlett Packard, Wilmington, DE). Ultrapure nitrogen was used as the carrier gas. The methodology of full evaporation technique (FET) was used [18]. This technique was based on a near-complete transfer of analytes from a condensed matrix into a vapor phase. Reproducible results were obtained by using 13 μl of sample in 22.5 ml headspace vial. The

Table 1
Characteristics of the module used

Module	Fiber substrate	Membrane coating	No. of fibers	OD (μm)	Active length (cm)	Mass-transfer area based on OD (cm^2)	Remarks
1	Celgard[a] (X-10)	Silicone[b]	75	290	20.5	140.1	Fabricated in lab

[a]Porosity (ε_m) is 0.4 and tortuosity (τ_m) is 2.49 [20].
[b]Plasma polymerized by AMT, Minnetonka, MN.

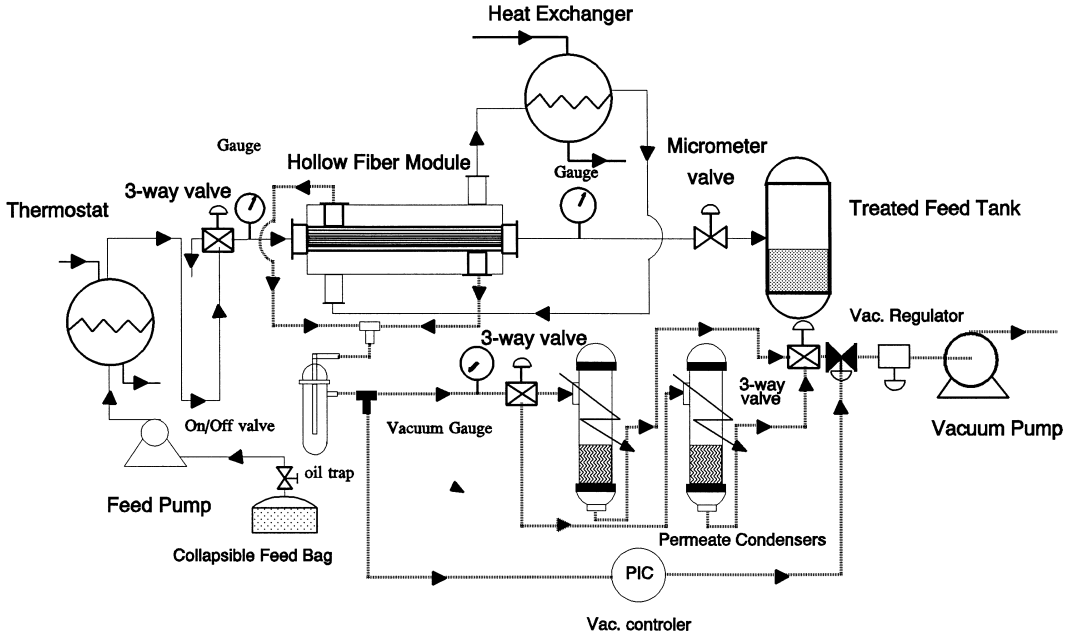

Fig. 2. Stripmeation experimental unit.

optimum headspace oven temperature (100°C), sample volume (13 μl) and sample equilibration time (5 min) were determined after an extensive study by varying each of these parameters one at a time. Sample vials were thermostated in the headspace analyzer for 5 min at 100°C. Headspace vapors were analyzed by pressurizing the vials for 0.15 min followed by a timed injection of the vapors for 1 min into the GC column. A temperature program was fixed to get clear separation of TCE. The initial oven temperature was set at 40°C for 1.5 min. In the next step, temperature was ramped at 25°C/min until it reached 75°C where it was kept for 1 min. In the final step, the temperature was ramped at 40°C/min until 160°C which was maintained for 3 min.

3.5. Experimental procedure

Fresh feed for an experiment was prepared before each experiment to avoid volatilization of TCE. The feed was prepared in a glass vessel with a minimum of headspace to avoid volatilization of TCE. Feed solution was pumped into the collapsible teflon bag which prevented formation of headspace during an experimental run and kept the feed concentration nearly constant. Feed was kept at a pressure range 7–10 psig by using a micrometering flow control valve (Swagelok, R.S. Crum, New Brunswick, NJ) in the retentate line. Feed pressure was monitored by using a dial pressure gauge (Cole Parmer, Vernon Hills, IL). Dewar flasks were filled with dry ice and methanol after putting in the condenser to achieve a low cooling temperature (approx. −50°C). The condenser and the feed lines were insulated with glasswool and aluminum foil. Samples were taken every half-hour and analyzed. The experiment generally reached steady state after 3 h and normal runs were carried out for 6–7 h. The experiment was stopped once consistent results were obtained from four consecutive samples. The volume of the permeate was observed and noted from the collection in the condenser. The volume of water and the VOC could be easily noted as the permeate separated into two distinct organic and aqueous phases. After every experiment the module was washed for a few hours with deionized water and filtered nitrogen was passed overnight to dry it before another experiment.

Sampling of feed and retentate in pervaporation experiments was done carefully to avoid any loss. The feed line was connected to a three-way valve for

the collection of the feed sample. At the time of the feed sample collection, the three-way valve was opened and the feed was allowed to flow for a minute to avoid any error arising from any stagnant feed in the collection line. Samples were collected in a small 2 ml glass vial and capped immediately with a teflon-lined cap to avoid TCE loss. For analysis in the GC/headspace, 13 μl of the sample was taken in a high precision Hamilton microsyringe and was directly injected into a headspace vial of volume 22.5 ml. Same procedure was followed for the retentate sample for the GC.

The experimental procedure for vapor permeation experiments will be briefly described now. A standard mixture of TCE in N_2 in a cylinder (Matheson, E. Rutherford, NJ) was passed through the tube side of module 1 at essential atmospheric pressure. A vacuum was maintained on the permeate side (shell side) at −29.2 in. Hg. The permeate flow was countercurrent with one end closed and the feed-side end connected to the vacuum pump. The gas flow rates at the inlet and the outlet were measured by electronic mass flow meters (Matheson, E. Rutherford, NJ). The composition of the gas stream at the feed outlet was measured in a Varian 3400 gas chromatograph (Varian Associates, Sugarland, TX) having a flame ionization detector; the column employed was a 0.3% Carbowax 20M, Carbopack C, Mesh 80/100, 0.85 in. ID, 0.1625 in. OD.

3.6. Calculated quantities

The fluxes of TCE and water were obtained, respectively, from the volumes of the TCE phase and water phase collected over time t from the membrane of area A_m:

$$J_i = \frac{V_{TCE}\rho_{TCE}}{A_m t}, \tag{15a}$$

$$J_w = \frac{V_{H_2O}\rho_{H_2O}}{A_m t}, \tag{15b}$$

where J_i and J_w are TCE flux and water flux, respectively.

Here A_m is defined as

$$A_m = \pi d_o N l, \tag{15c}$$

where N is the number of hollow fibers of outside diameter d_o and length l. The Reynolds number for the flow inside the fiber is defined by

$$Re = \frac{d_i \rho_{H_2O} v}{\mu_{H_2O}}, \tag{16}$$

where the velocity of the solution v is obtained from

$$v = \frac{4Q}{60N\pi d_i^2} \tag{17}$$

for a volumetric flow rate of Q (cm^3/min). The overall mass-transfer coefficient K_o for TCE is obtained from

$$J_i = K_o \Delta C_{lm}, \tag{18}$$

where ΔC_{lm} is obtained from

$$\Delta C_{lm} = \frac{(C_{inlet} - C^p_{inlet}) - (C_{outlet} - C^p_{outlet})}{\ln[(C_{inlet} - C^p_{inlet}/(C_{outlet} - C^p_{outlet})]}. \tag{19}$$

We have assumed that C^p_{inlet} as well as C^p_{outlet} may be neglected in comparison to C_{inlet} and C_{outlet}, respectively. We will show here that the K_o of Eq. (18) under such conditions is essentially identical to K_o of Eq. (4). Since $C^p_{inlet} \ll C_{inlet}$ and $C^p_{outlet} \ll C_{outlet}$, we can in the same spirit assume $C''_{ipl} \ll C'_{il}$ in Eq. (4) and obtain

$$R_i = K_o \pi d_o C'_{il}. \tag{20a}$$

Integrating along the module length and assuming that this K_o is a constant, we get from Eqs. (4) and (18)

$$J_i \pi d_o = (1/l) \int_0^l R_i \, dl = [(K_o \pi d_o)/l] \int_0^l C'_{il} \, dl. \tag{20b}$$

If we replace the integral on the right hand side by its logarithmic average, namely, $l[(C_{inlet} - C_{outlet})]/\ln[C_{inlet}/C_{outlet}]$ we observe that K_o of Eq. (4) is the same as the K_o of Eq. (18).

The Sherwood number is defined as

$$Sh = \frac{K_o d_o}{D_{il}}, \tag{21a}$$

where D_{il} is the diffusivity of TCE in water. Percent removal of TCE is defined as

$$\text{removal } (\%) = \frac{C_{inlet} - C_{outlet}}{C_{inlet}} \times 100. \tag{21b}$$

The value of $k_m m_{vf}$ was obtained from vapor permea-

tion experiments via the following definition:

$$J_i^{\mathrm{v}} = m_{vf} k_{\mathrm{m}} \Delta C_{\mathrm{lm}}^{\mathrm{v}}, \tag{22}$$

where J_i^{v} is the permeate flux and $\Delta C_{\mathrm{lm}}^{\mathrm{v}}$ is defined by

$$\Delta C_{\mathrm{lm}}^{\mathrm{v}} = \frac{(C'_{\mathrm{inlet}} - C''_{\mathrm{inlet}}) - (C'_{\mathrm{outlet}} - C''_{\mathrm{outlet}})}{\ln[(C'_{\mathrm{inlet}} - C''_{\mathrm{inlet}})/(C'_{\mathrm{outlet}} - C''_{\mathrm{outlet}})]}. \tag{23}$$

4. Results and discussion

We will first illustrate the performance of a hollow fiber module (module 1) at 25°C as the feed TCE concentration was changed at a low feed flow rate of 2.5 ml/min. Fig. 3 shows that % TCE removal is reasonably constant with increasing TCE concentration. The TCE flux appears to be linear with the TCE concentration in the feed. Fig. 4 illustrates the TCE removal behavior for feed TCE concentrations in the range 800–900 ppm at a number of high flow rates. Obviously, due to the limited amount of membrane area in module 1, the extent of removal of TCE is drastically reduced as the feed flow rate is increased. For example, the percent TCE removal drops from 80% at 5 ml/min to about 13% at 105 ml/min. This leads to a much higher TCE concentration throughout the module and correspondingly the TCE flux appears to increase almost linearly with the feed flow rate. The water flux should be unaffected by the feed flow rate; the experimental results confirm it.

The mass-transfer coefficient of TCE based on definition (18) and the logarithmic concentration difference (19) has been plotted in Fig. 5 as a function of the fiber bore Reynolds number. In the same figure, we have also plotted the mass-transfer coefficient according to the Graetz solution (14). The data were obtained from module 1 at 25°C in the TCE concentration range 700–900 ppm; the data shown in Fig. 4 along with the others not shown were utilized to obtain this plot. It is clear that the observed total resistance is significantly larger than that due to the feed solution boundary layer resistance in the fiber bore (Graetz solution (14) is used here to obtain a working estimate of the latter). Eq. (13) would suggest this to be due to the silicone membrane resistance. We test this aspect in Fig. 6.

Fig. 6 plots first the overall mass-transfer coefficient data of TCE obtained using ΔC_{lm} of Eq. (19) as the Sherwood number $(N_{\mathrm{Sh}})_{\mathrm{lm}}$ against the Graetz number. The Sherwood number for Graetz solution corresponding to constant wall concentration [16] is also plotted in the same figure as a solid line for $(N_{\mathrm{Sh}})_{\mathrm{lm}}$ versus Graetz number. The difference between the two appears to be rather constant independent of

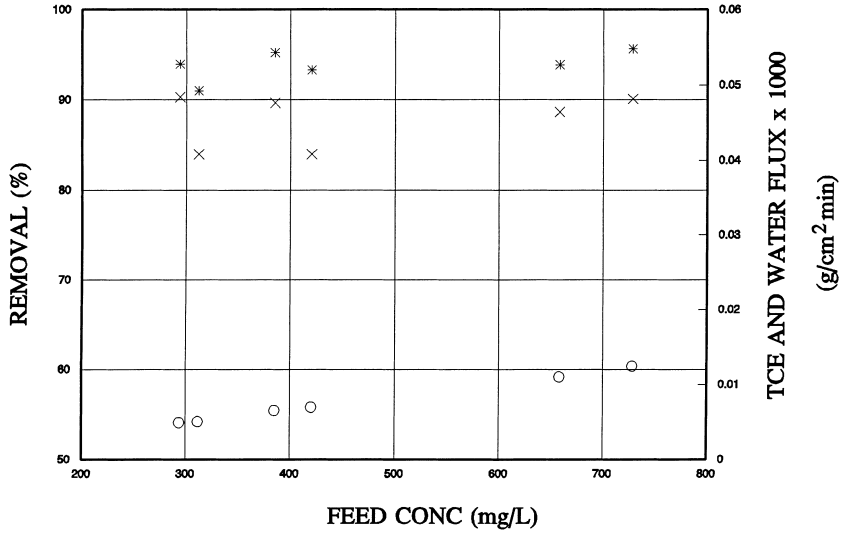

Fig. 3. TCE removal, TCE flux and water flux in stripmeation process: flow rate=2.5 ml/min; vacuum=20 Torr; A_{m}=140.1 cm^2; TCE=280–800 ppm; once-through mode. (*) Removal, (○) TCE flux, (×) water flux.

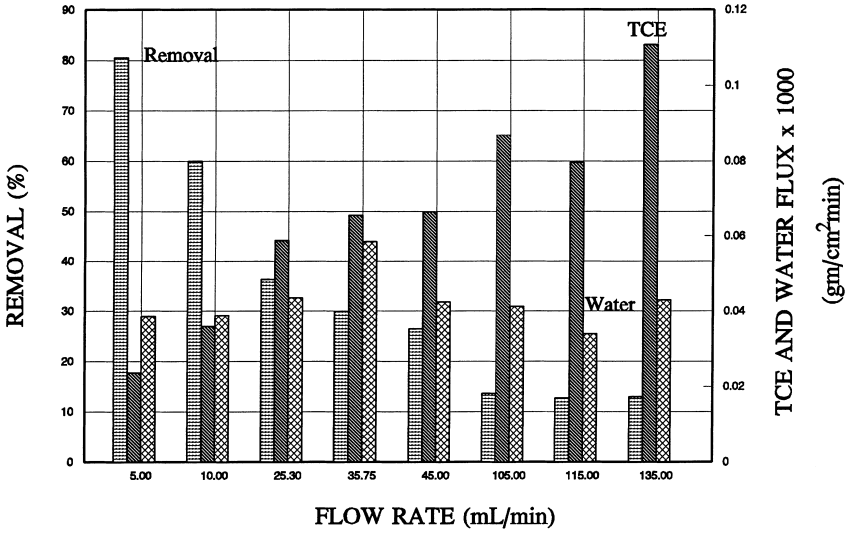

Fig. 4. Effect of feed flow rate on TCE removal, TCE flux and water flux: TCE concentration=800–900 ppm; vacuum=20 Torr; A_m=140.1 cm^2; single module feed–bleed mode.

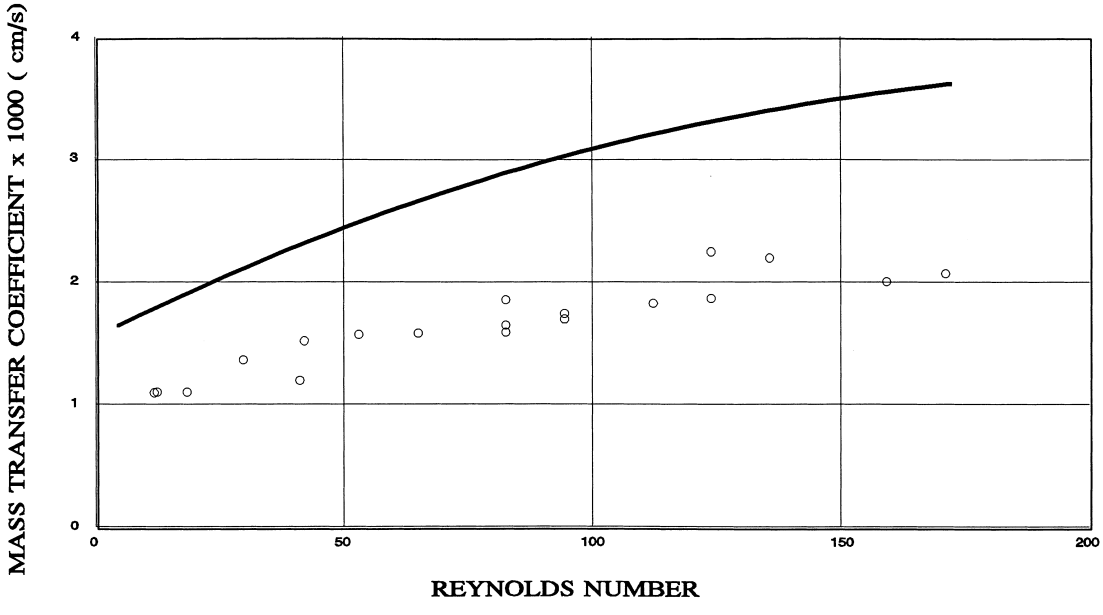

Fig. 5. Effect of hydrodynamics on TCE overall mass-transfer coefficient: TCE/water system; TCE concentration=800–900 ppm; vacuum=20 Torr; A_m=140.1 cm^2; feed–bleed mode. (———) Graetz; (○) experimental.

the Graetz number. We now want to show that this difference reflects the silicone membrane resistance.

From Table 2 where we have provided the experimental data and calculated quantities (see Appendix A for details) for the vapor permeation experiments with TCE in N_2 for a number of feed TCE concentrations (220–935 ppm), we observe that the value of $k_m m_{vf}$ in the vapor permeation equation,

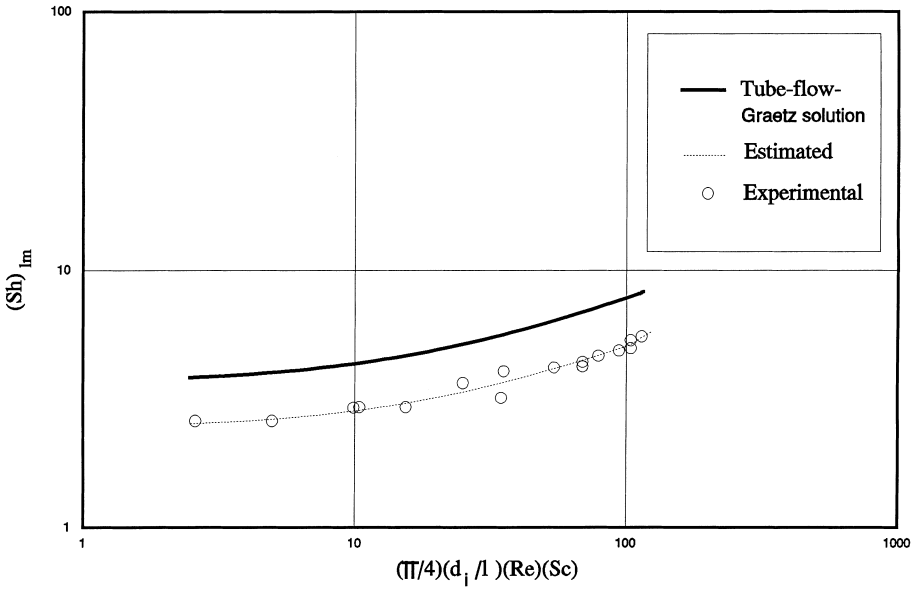

Fig. 6. Comparison of experimentally obtained TCE overall mass-transfer coefficient with model-estimated values.

Table 2
Results of vapor permeation experiments and simulations with TCE in N_2

Module	Flow rate (cm^3/min)		TCE concentration (ppmv)		Simulated TCE concentration (mole fraction)		ΔC_{lm} ($\times 10^8$ g mol/cm^3)	TCE flux ($\times 10^{10}$ g mol/ cm^2 s)	$k_m m_{vf}$ (cm/s)
	Feed in	Feed out	Feed in	Feed out	Closed end	Permeate out			
1	214.8	207.0	220	141	0.0022	0.0029	0.50	0.96	0.019
1	419.0	405.2	467	376	0.0061	0.0070	1.14	2.31	0.0201
1	306.3	297.7	631	467	0.0093	0.0110	1.29	2.89	0.0223
1	347.8	339.6	751	567	0.0075	0.0091	1.99	3.65	0.0183
1	352.9	346.2	867	656	0.0108	0.0127	2.06	4.20	0.0204
1	272.9	267.0	935	641	0.0106	0.0132	2.14	4.46	0.0209

Eq. (22), for TCE flux, J_i^v (where we have assumed m_{vf}=m_{vp} which is quite reasonable for this dilute system) is around 0.02 cm/s. Since the value of H_i for TCE is 2.75 $(mg/l)_{liq}/(mg/l)_{vap}$ [15], we get a value of 131.5 s/cm for $(H_i/m_{vf}k_m)$ in Eq. (13). Using this estimate in Eq. (13) and the value of k_l^f from the $(Sh)_{lm}$ versus Graetz number valid for Gratez solution (14) for tube flow, we have plotted a dotted line for the estimated value of K_o, the overall mass-transfer coefficient, in Fig. 6. As one can see, the difference between the estimated K_o and the experimentally obtained K_o is minor; the standard deviation in *Sh* was estimated to be 0.17. This agreement, then, provides a fundamental basis for determining the values of K_o in the proposed "stripmeation" process for removing VOC from an aqueous solution through the substrate side of the coated hollow fiber.

Amongst a number of other aspects of interest in this process, we focus on one particular aspect now. How does the "stripmeation" process work vis-à-vis the conventional pervaporation process with such hollow fiber membranes? Fig. 7 provides experimen-

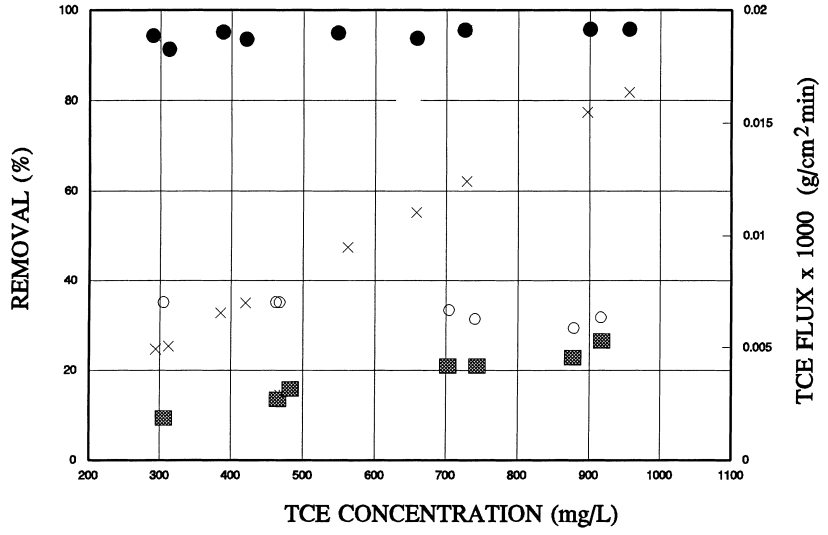

Fig. 7. TCE removal and TCE flux-comparison of tube-side and shell-side results: TCE/water system; TCE concentration=280–980 ppm; flow rate=2.5 ml/min; vacuum=20 Torr; A_m=140.1 cm^2; once-through mode. (●) Removal/tube; (×) TCE flux/tube; (○) removal/shell; (■) TCE flux/shell.

tal data on the removal and flux of TCE when the feed solution was passed on the shell side; this mode of operation was simple pervaporation where the membrane was in direct contact with the feed liquid. The aqueous feed solution flow rate was the same as in Fig. 3, namely, 2.5 ml/min. For the sake of comparison, the data from Fig. 3 are also plotted here. It appears that the TCE removal is substantially lower

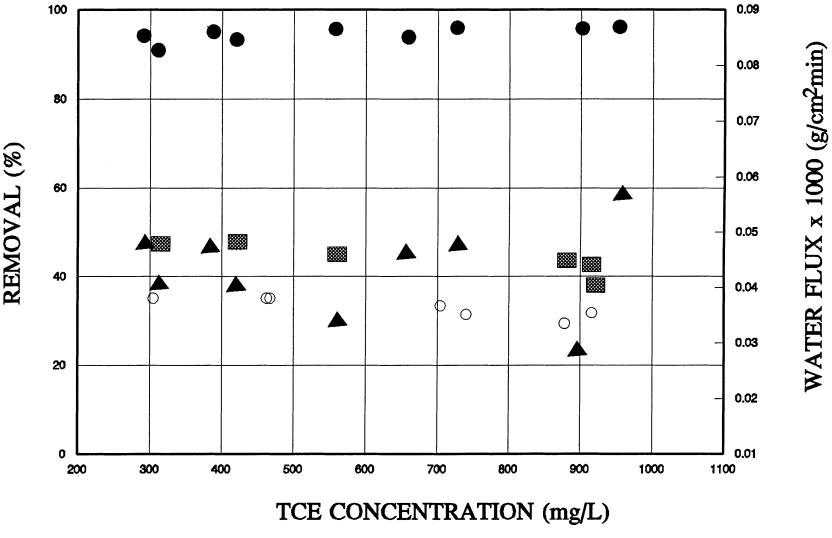

Fig. 8. TCE removal and water flux-comparison of tube-side and shell-side results: TCE/water system; TCE concentration=280–980 ppm; flow rate=2.5 ml/min; vacuum=20 Torr; A_m=140.1 cm^2; once-through mode. (●) Removal/tube; (▲) water flux/tube; (○) removal/shell; (■) water flux/shell.

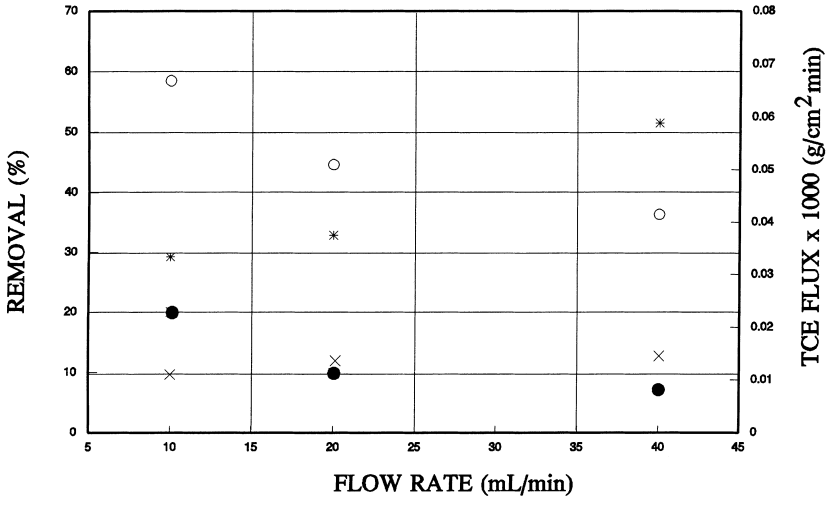

Fig. 9. Effect of hydrodynamics on TCE removal and TCE flux for feed on shell side: TCE/water system; TCE concentration=700–800 ppm; vacuum=20 Torr; A_m=40.1 cm^2; feed–bleed mode. (●) Removal/shell; (×) TCE flux/shell; (○) removal/tube; (∗) TCE flux/tube.

when the feed is on the shell side. In fact the % removal of TCE for the feed flow on the shell side is almost half of that for flow on the tube side. This figure also shows the corresponding fluxes of TCE in the two flow configurations. The tube side flux of TCE is, as expected, considerably larger than that in the shell side. The values for water flux for flow in the tube side and shell side are shown in Fig. 8. They are comparable to each other.

Figs. 9 and 10 illustrate the effect of hydrodynamics on TCE removal, TCE flux and water flux when the feed is passed on the shell side. Corresponding results for experiments with feed in the tube side have also been plotted. Flow rate was varied between 10 and 40 ml/min. TCE concentration was in the range 800–900 ppm similar to that for the tube-side experiments. It is evident (Fig. 9) that TCE removal and TCE flux are much lower for feed in the shell side

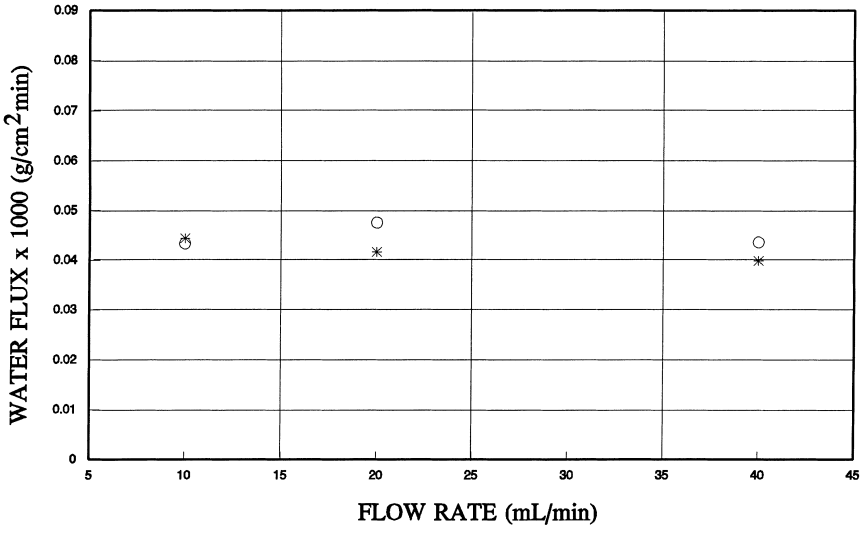

Fig. 10. Effect of hydrodynamics on water flux for feed on shell side: TCE/water system; TCE concentration=700–800 ppm; vacuum=20 Torr; A_m=140.1 cm^2; feed–bleed mode. (∗) Water flux/shell; (○) water flux/tube.

compared to feed in the tube side. Water flux seems unaffected by change in feed flow rate and has values comparable to tube-side feed (Fig. 10).

A number of different arguments are useful here. In the conventional pervaporation mode, there is a considerable pressure drop in the substrate pores and the tube side when vacuum is applied to the tube side. The corresponding pressure drops in the tube-side feed in ''stripmeation'' is essentially nonexistent since the shell side is highly open. However, the shell-side velocity is much lower than that on the tube side due to the much larger open area. Further there are considerable possibilities for bypassing on the shell side. The very low values of the feed flow rate and the highly open structure of the shell side (high void volume and widely distributed fibers) do, however, reduce the extent and effect of ''bypassing'' considerably.

5. Concluding remarks

The ''stripmeation'' process for removing VOCs from an aqueous solution has been described. Such a process was shown to remove TCE successfully from an aqueous solution. This process is based on the stripping of TCE into a gas-filled pore of a hydrophobic membrane and then vapor permeation of the TCE through a silicone coating on the fiber outside diameter subjected to a vacuum was shown to be significantly more efficient than conventional pervaporation where the feed solution was directly imposed on the silicone membrane on the fiber outside diameter. The mass-transfer rate in the ''stripmeation'' process may be reasonably described by a four resistances-in-series model where the vapor permeation resistance of the silicone membrane and the tube-side aqueous boundary layer are the controlling resistances.

6. Notation

A_m membrane area based on fiber outside diameter (cm^2)

B_j coefficient in the jth term of an infinite series [16]

$\bar{c}_i$ mean speed of molecules (cm/s)

C'_{il} bulk phase feed concentration of species i (g mol/cm^3)

C'_{ili} concentration of species i in the aqueous feed phase at the aqueous–pore gas interface (g mol/cm^3)

C'_{igi} concentration of species i in the vapor phase at the aqueous–pore gas interface (g mol/cm^3)

C'_{igmi} concentration of species i in the vapor phase at the pore gas–silicone membrane interface (g mol/cm^3)

C'_{imi} concentration of species i in the membrane at the pore gas–silicone membrane interface (g mol/cm^3)

C''_{imi} concentration of species i in the membrane at the silicone membrane–vacuum side interface (g mol/cm^3)

C''_{imp} concentration of species i in the vacuum side at the silicone membrane–vacuum side interface (g mol/cm^3)

C''_{ip} bulk concentration of species i in the vacuum side (g mol/cm^3)

C''_{ipl} hypothetical equilibrium liquid phase concentration in equilibrium with the vacuum side gas phase (g mol/cm^3)

C_{inlet} feed aqueous inlet concentration of TCE (g mol/cm^3)

C_{outlet} feed aqueous outlet concentration of TCE (g mol/cm^3)

$C^{\text{p}}_{\text{inlet}}$ hypothetical permeate aqueous concentration of TCE at feed inlet location in equilibrium with the vacuum phase (g mol/cm^3)

$C^{\text{p}}_{\text{outlet}}$ hypothetical permeate aqueous concentration of TCE at feed outlet location in equilibrium with the vacuum phase (g mol/cm^3)

ΔC_{lm} logarithmic mean aqueous concentration of TCE as defined by Eq. (19) (g mol/cm^3)

C'_{inlet} feed gas inlet concentration of TCE (g mol/cm^3)

C'_{outlet} feed gas outlet concentration of TCE (g mol/cm^3)

C''_{inlet} permeate vapor concentration of TCE at feed inlet (g mol/cm^3)

C''_{outlet} permeate vapor concentration of TCE at feed outlet location (g mol/cm^3)

$\Delta C^{\text{v}}_{\text{lm}}$ logarithmic mean vapor concentration of TCE as defined by Eq. (23) (g mol/cm^3)

d_i inner diameter of Celgard hollow fiber (cm)
d_o outer diameter of Celgard hollow fiber (cm)
d_{lm} logarithmic mean diameter of Celgard hollow fiber, $(d_o - d_i)/\ln(d_o/d_i)$ (cm)
D_{igp} diffusion coefficient of TCE in the gaseous pore (cm^2/s)
D_{il} diffusion coefficient of TCE in water (cm^2/s)
H_i Henry's law constant for species i defined by Eq. (1) $(mg/l)_{liq}/(mg/l)_{vap}$
J_i permeation flux of species i (g mol/cm^2 min)
J_i^v permeation flux of species i in vapor permeation experiments (g mol/cm^2 min)
J_w permeation flux of water (g mol/cm^2 min)
K_o overall mass-transfer coefficient defined by Eq. (4) (cm/s)
k_g^p vacuum side mass-transfer coefficient (cm/s)
k_{gp}^f mass-transfer coefficient for mass transfer across the gas-filled pore (cm/s)
k_l^f aqueous phase mass-transfer coefficient for mass transfer across the feed side boundary layer (cm/s)
k_m mass-transfer coefficient for mass transfer across the membrane (cm/s)
l active length of the module (cm)
m_{vp} distribution coefficient of TCE between the vacuum side and the membrane
m_{vf} distribution coefficient of TCE between the membrane and the gaseous phase
M_i molecular weight of species i
N number of hollow fibers
Q volumetric flow rate (cm^3/min)
r_i radius of a tube (cm)
R_i permeation rate of species i per unit permeator length (g mol/cm s)
Re Reynolds number as defined by Eq. (16)
Sc Schmidt number defined as $\mu_i/\rho_i D_v$
Sh Sherwood number as defined by Eq. (21a)
t time (s)
v linear velocity of the feed (cm/s)
V_{TCE} volume of TCE collected (cm^3)
V_{H_2O} volume of water collected (cm^3)

Greek symbols

δ_s fiber substrate thickness (cm)
ϵ porosity of the Celgard fibers
τ tortuosity of pores in the Celgard fibers
π 3.1416
ρ_{H_2O} density of water (g/cm^3)
ρ_{TCE} density of TCE (g/cm^3)
μ_{H_2O} viscosity of water (g/cm s)

Acknowledgements

This research was conducted under the SERDP program (EPA-371-94) administered through the EPA Northeast Hazardous Substance Research Center at Newark, NJ 07102. The supply of coated fibers by AMT is gratefully acknowledged.

Appendix A

The method by which the permeance of TCE has been determined from the vapor permeation experiments is based on detailed experimental studies and numerical modeling by Cha et al. [19] using similar hollow fiber membranes. Cha et al. [19] had developed a set of equations to describe vapor permeation under identical physical conditions. The equations were solved numerically for a given expression of permeance of a VOC as a function of the VOC partial pressure on the feed side. It is known from these and other studies for at least four different VOCs (e.g. methanol, toluene, methylene chloride and acetone) that at VOC concentrations of 200–1000 ppmv, the permeance is essentially constant. For the set of experiments conducted for this study, TCE concentration in the feed ranged between 220 and 935 ppmv. The procedure followed was as follows. The TCE inlet concentration in the feed and the feed flow rate at the inlet were fed into the numerical model. A value of $k_m m_{vf}$ was calculated using ΔC_{lm} value for the gas phase for a given experiment by neglecting the partial pressure of TCE on the permeate side. This value was used as a starting guess for the iteration. The numerical solution of the model provided as output the TCE outlet concentration in the feed, the feed flow rate at the outlet and the permeate side partial pressure profile of TCE. The TCE outlet concentration in the feed and the feed flow rate at the outlet were matched to the experimental data; if the simulated results were found to be reasonably close to experimental results, the permeate side partial pressures and the corresponding concentrations were used in Eq. (23) to calculate the

value of $k_m m_{vf}$ from Eq. (22). If the simulated results showed significant divergence from the experimental results, the procedure was repeated until satisfactory convergence was achieved.

References

[1] R.Y.M. Huang (Ed.), Pervaporation Membrane Separation Processes, Elsevier, Amsterdam, 1991.

[2] C.S. Slater, H. Fleming, Pervaporation, in: W.S. Winston Ho, K.K. Sirkar (Eds.), Membrane Handbook, Chapters 7–10, Chapman&Hall, New York, 1992.

[3] J.G. Wijmans, A.L. Athayde, R. Daniels, J.H. Ly, H.D. Kamaruddin, I. Pinnau, The role of boundary layers in the removal of volatile organic compounds from water by pervaporation, J. Membr. Sci. 109 (1996) 135.

[4] X. Feng, R.Y.M. Huang, Liquid separation by membrane pervaporation: a review, Ind. Eng. Chem. Res. 36 (1997) 1048.

[5] C.H. Gooding, P.J. Hickey, M.L. Crowder, Mass transfer characteristics of a new pervaporation module for water purification, in: R. Bakish (Ed.), Proceedings of the Fifth International Conference on Pervaporation Processes in Chemical Industry, Bakish Materials, Englewood, NJ, 1991, pp. 237–249.

[6] X. Feng, R.Y.M. Huang, Permeate pressure buildup in the shellside-fed hollow fiber pervaporation membrane, Can. J. Chem. Eng. 73 (1995) 833.

[7] R.Y.M. Huang, X. Feng, Resistance model approach to asymmetric polyetherimide membranes for pervaporation of isopropanol/water mixtures, J. Membr. Sci. 84 (1993) 15.

[8] D. Yang, S. Majumdar, S. Kovenklioglu, K.K. Sirkar, Hollow fiber contained liquid membrane pervaporation system for the removal of toxic volatile organics from wastewater, J. Membr. Sci. 103 (1995) 195.

[9] C. Lipski, P. Cote, The use of pervaporation for the removal of organic contaminants from water, Environ. Progr. 9 (1990) 254.

[10] T. Uragami, M. Saito, Analysis of permeation and separation characteristics and new techniques for separation of aqueous alcoholic solutions through alginic acid membranes, Sep. Sci. Technol. 31 (1990) 668.

[11] T. Uragami, H. Shinomiya, Concentration of aqueous dimethyl sulfoxide solutions through a chitosan membrane by permeation with a temperature difference, J. Membr. Sci. 74 (1992) 183.

[12] M.J. Semmens, R. Qin, A. Zander, Using a microporous hollow-fiber membrane to separate VOCs from water, J. AWWA (1989) 162.

[13] R. Rangarajan, M.A. Mazid, T. Matsuura, S. Sourirajan, Permeation of pure gases under pressure through asymmetric porous membranes: membrane characterisation and prediction of performance, Ind. Eng. Chem. Process Des. Dev. 23 (1984) 79.

[14] R.W. Callahan, Novel uses of microporous membranes: a case study, AIChE Symp. Ser. (no. 261) 84 (1988) 54.

[15] L.H. Turner, Y.C. Chiew, R.C. Ahlert, D.S. Kosson, Measuring vapor–liquid equilibrium for aqueous–organic systems: review and a new technique, AIChE J. 42 (1996) 6.

[16] A.H.P. Skelland, Diffusional Mass Transfer, Wiley, New York, 1974, pp. 158–160.

[17] S. Chandra, Removal of volatile organic compounds from contaminated ground water by pervaporation, M.S. Thesis, New Jersey Institute of Technology, Newark, NJ, 1996.

[18] M. Markelov, J.P. Guzowski Jr., Matrix independent headspace gas chromatographic analysis. The full evaporation technique, Anal. Chim. Acta 15 (1993) 234–245.

[19] J.S. Cha, V. Malik, D. Bhaumik, R. Li, K.K. Sirkar, Removal of VOCs from waste gas streams by permeation in a hollow fiber permeator, J. Membr. Sci. 128 (1997) 195.

[20] R. Prasad, K.K. Sirkar, Dispersion free solvent extraction with microporous hollow fiber modules, AIChE J. 34 (1988) 177.